International Journal of Peptide Research and Therapeutics (2022) 28: 129
https://doi.org/10.1007/s10989-022-10441-x

BRIEF REPORT

A Model Peptide Reveals Insights into the Interaction of Human Hemopexin with Heme

Marie-T. Hopp[1] · Ajay A. Paul George[2] · Anuradha Ramoji[3,4,5] · Anna Pepanian[1] · Milena S. Detzel[1] · Ute Neugebauer[3,4,5] · Diana Imhof[1]

Accepted: 3 July 2022 / Published online: 18 July 2022

Abstract

Under hemolytic conditions, toxic heme is scavenged by hemopexin. Recently, the heme-binding properties of hemopexin have been reassessed, which revealed a K_D of ~ 0.32 nM as well as a stoichiometry of one to two heme molecules binding to hemopexin. A 66mer hemopexin-derived peptide that spans over three heme-binding motifs was used to verify the earlier suggested heme-recruiting mechanism. Herein, we employed spectroscopic and computational methods to substantiate the hypothesis of more than one heme molecule binding to hemopexin and to analyze the heme-binding mode. Both, hemopexin and the 66mer peptide, were found to bind heme in mixed penta- and hexacoordinated states, which strongly indicates that heme binding follows distinct criteria and increases rigidity of the peptide-heme complex. Additional in silico molecular dynamics simulations support these experimental findings and, thus, contribute to our understanding of the molecular basis of the heme-hemopexin interaction. This analysis provides further details for consideration of hemopexin in biomedical applications.

Keywords 66mer peptide · Heme · Hemolysis · Hemopexin · Hemopexin-derived peptide · rRaman

Introduction

Under hemolytic conditions, the plasma level of labile heme (Fe(II/III) protoporphyrin) can reach tremendous pathological concentrations due to premature lysis of red blood cells and subsequent heme release from hemoglobin (Hb) after its oxidation to met-Hb (ferrihemoglobin) (Kumar and Bandyopadhyay 2005; Dutra et al. 2014; Roumenina et al. 2016).

Marie-T. Hopp and Ajay A. Paul George contributed equally.

✉ Diana Imhof
dimhof@uni-bonn.de

[1] Pharmaceutical Biochemistry and Bioanalytics, Pharmaceutical Institute, University of Bonn, Bonn, Germany

[2] BioSolveIT GmbH, Sankt Augustin, Germany

[3] Leibniz Institute of Photonic Technology Jena, Jena Biophotonics and Imaging Laboratory, Jena, Germany

[4] Center for Sepsis Control and Care, Jena University Hospital, Jena, Germany

[5] Institute of Physical Chemistry and Abbe Center of Photonics, Friedrich Schiller University, Jena, Germany

The released heme is first bound to albumin, as it is the most abundant protein in human plasma (~ 600 µM), and is then transferred to hemopexin (Morgan et al. 1976; Peters 1996; Paoli et al. 1999; Tolosano et al. 2010). In most severe cases of hemolysis, heme levels overwhelm the heme-scavenging capacity of plasma, thus provoking proinflammatory, procoagulant, and cytotoxic effects either due to heme-driven production of reactive oxygen species and damage of proteins, lipids, and nucleic acid, or through direct interaction with proteins of the complement and the blood coagulation system (Kumar and Bandyopadhyay 2005; Roumenina et al. 2016; Frimat et al. 2019; Hopp and Imhof 2021).

Circulating in the blood stream in a concentration of ~ 17 µM, hemopexin serves as the high-affinity heme scavenger in the blood stream. Human hemopexin is a ~ 57 kDa glycoprotein consisting of 439 amino acids organized in two domains that are connected via a flexible linker peptide (Hrkal et al. 1974; Takahashi et al. 1985; Paoli et al. 1999; Tolosano and Altruda 2002). It enables the transport of heme to its degradation site, i.e. hepatocytes (Smith and Morgan 1981; Hvidberg et al. 2005; Tolosano et al. 2010). There, the hemopexin-heme complex binds to the low density lipoprotein receptor-related protein 1 (LRP1/CD91) and is taken up

by the cells (Smith and Morgan 1981; Hvidberg et al. 2005; Tolosano et al. 2010). Based on this function of the protein, exogenously administered hemopexin has just recently been proven to protect from the toxic heme-triggered effects and their consequences (e.g., vasoocclusion, kidney and brain injury) in hemolytic and hemorrhagic disorders, such as sickle cell disease and intracerebral hemorrhage, respectively (Belcher et al. 2018; Poillerat et al. 2020; Chen-Roetling et al. 2021; Buehler et al. 2021; Buzzi et al. 2021). Thus, a plasma-derived form of hemopexin ("CSL889") as developed by CSL Behring is currently in phase 1 clinical trial (ClinicalTrials.gov identifier: NCT04285827) for the treatment of sickle cell disease in adults.

The interaction between hemopexin and heme has been characterized almost 50 years ago and defined as one of the high-affinity protein–ligand complexes with a $K_D < 1$ pM (Hrkal et al. 1974). Recent investigations employing surface plasmon resonance (SPR) spectroscopy, however, revealed a much lower affinity ($K_D \sim 0.32$ nM) (Detzel et al. 2021). By using SPR analysis and ultraviolet–visible (UV/Vis) spectroscopic titration a binding stoichiometry of 1:1 to 1:2 (hemopexin:heme) has been determined (Detzel et al. 2021), which was later discussed by Karnaukhova et al. as well (Karnaukhova et al. 2021). As explored in the crystal structure of the rabbit hemopexin-heme complex, hemopexin binds heme in a hexacoordinated state by two histidine residues (H^{236} and H^{293}) (Paoli et al. 1999). However, in total, a number of five heme-binding sites were suggested by different groups until 1999 (Morgan et al. 1993; Satoh et al. 1994; Paoli et al. 1999). Recently, these potential heme interaction sites, hereinafter referred to as heme-binding motifs (HBMs), were narrowed down to four histidine residues (H^{79}, H^{105}, H^{236}, and H^{293}) (Detzel et al. 2021). In addition, a HeMoQuest analysis revealed so far unconsidered histidine residues (i.e. H^{238} and H^{260}) for potential heme binding (Paul George et al. 2020; Detzel et al. 2021). As already demonstrated and proven for several other proteins (Kühl et al. 2013; Brewitz et al. 2016; Peherstorfer et al. 2018; Wißbrock et al. 2019a; Hopp et al. 2021), the heme-binding capacity of the suggested HBMs (in form of nonapeptides) was analyzed by UV/Vis spectroscopy, which provided experimental verification of heme binding to these HBMs for the first time (Detzel et al. 2021). The presence of HBMs with an even higher heme-binding affinity than the earlier described HBM in the crystal structure, suggested an intramolecular recruitment mechanism of heme from the protein's surface to the actual heme-binding site between H^{236} and H^{293} (Detzel et al. 2021). Thus, the two "big unknowns" in hemopexin-related research include (a) the structure of the human hemopexin-heme complex (so far only an incomplete structure of rabbit hemopexin is available from 1999 (Paoli et al. 1999)), and (b) the confirmation of the suggested heme-recruitment mechanism (Detzel et al. 2021). This lack of information prompted us to examine the binding mode of the heme molecules in hemopexin more closely. From a clinical point of view, this information is also highly relevant for biomedical applications of hemopexin in the context of a supplemental therapy in hemolytic conditions associated with high heme levels.

Herein, we used an in-house synthesized 66mer hemopexin-derived peptide (P^{232} to I^{297}) representing the linker peptide (P^{232} to P^{252}) and a part of the C-terminal domain (E^{253} to I^{297}) of hemopexin, which spans over the confirmed heme-binding sites H^{236} and H^{293} as well as the suggested H^{260} (Paoli et al. 1999; Detzel et al. 2021). The heme-binding behavior was investigated at different ratios of peptide and heme using resonance Raman (rRaman) and circular dichroism (CD) spectroscopy. In addition, we performed the rRaman study with full-length human hemopexin to compare the results obtained on the peptide level with those from the protein level. Substantial molecular dynamics (MD) simulations provide insights into the structure of the complex and its binding mode. The results of the present study further substantiate the fact that hemopexin can bind two heme molecules at the same time, which is relevant concerning clinical dose calculations prior to application in patients in the future.

Materials and Methods

Characterization of the 66mer Hemopexin-Derived Peptide

The earlier synthesized 66mer hemopexin-derived peptide (Detzel et al. 2021) was analytically characterized by means of reversed-phase high-performance liquid chromatography (RP-HPLC) on a LC-10AT system (Shimadzu) equipped with a Vydac 218 TP column (C18, 250 × 4.6 mm, 5 µm particle size, 300 Å pore size), electrospray ionization mass spectrometry (ESI–MS) with a micrOTOF-QIII system (Bruker Daltonics), and amino acid analysis using a LC 3000 (Eppendorf-Biotronik) with a cation exchange column (CK10 M resin, 4 µm particle size, 10% cross-linkage, type H; Mitsubishi) and post-column derivatization with ninhydrin.

rRaman Spectroscopy

The rRaman spectra were acquired with a micro-Raman setup (CRM 300, WITec GmbH, Germany). The preparation of the respective peptide-heme complexes has been described earlier (Detzel et al. 2021). The exact concentration of the freshly prepared heme stock solutions (1 mM in 30 mM NaOH) was determined after dilution to 10 µM in HEPES buffer (100 mM, pH 7.4) using the molar extinction

coefficient $\varepsilon_{398} = 32.6\ mM^{-1}\ cm^{-1}$ (Hopp et al. 2020). Hemopexin, isolated from human plasma, was purchased from Athens Research & Technology. rRaman measurements were performed as previously described (Kühl et al. 2013; Brewitz et al. 2016; Syllwasschy et al. 2020), except for the fact that herein a peptide:heme ratio of 1:2 was applied. The samples were measured in liquid phase using a Zeiss 10× objective (NA 0.2, laser power 22 mW). The hemopexin sample was placed on an in-house built rotating sample holder (speed: 1 rotation/min). Precipitated samples were resuspended before measurement. The excitation wavelength was 405 nm. A CCD camera (DV401A BV-532, ANDOR, 1024 × 127 pixels) and a grating of 1800 g/mm was used for the fitting of the spectrometer. rRaman spectra were collected in triplicates with 30 s integration time per spectrum and the background noise was corrected using the statistics-sensitive non-linear iterative peak-clipping (SNIP) algorithm (Ryan et al. 1988). For analysis, the GNU R platform (R Core Team 2021) and an in-house built script were applied. The spectral regions of interest (600–900 cm^{-1} and 1400–1800 cm^{-1}) were plotted with GraphPad Prism 9.1.0.

CD Spectroscopy

CD spectroscopy measurements were performed on a JASCO J-715 spectropolarimeter at a constant temperature of 20 °C. The spectra were recorded with a scan speed of 100 nm/min, a band width of 1.00 nm, an accumulation of 5 scans, and a resolution of 0.20 nm. A 1 mm quartz cuvette was used, and the spectra were recorded from 180 to 350 nm. Basis line correction was performed with the spectrum of a 50 mM sodium phosphate buffer (pH 7.4) and the ellipticity of the CD spectra was expressed in millidegrees and later converted to molar ellipticity (θ) in $deg*cm^2*dmol^{-1}$. A stock solution of hemin (2 mM in 30 mM sodium hydroxide) was diluted to 75 µM (for peptide:heme ratio 1:1) and 150 µM (for peptide:heme ratio 1:2) in 50 mM sodium phosphate buffer (pH 7.4), respectively. 200 µL of each of the diluted solutions were added to an aliquot of the 66mer peptide (final concentration: 75 µM). Experimental set-up was adapted from earlier performed measurements (Kühl et al. 2011; Fleischhacker et al. 2020). The spectra were recorded after 30 min incubation time and evaluated as well as presented with GraphPad Prism 9.1.0.

In Silico Docking and Molecular Simulation Studies

The 66mer peptide was subjected to an all-atom MD simulation study. The earlier reported structure of the 66mer peptide (Detzel et al. 2021) was used as the starting structure for the MD simulation. The resulting initial structure was obtained with a good overall Z-score of 0.60 in YASARA (version 20.4.20) (Krieger and Vriend 2014). This structure was subjected to a 2000 ns MD simulation at pH 7.4 and 298 K using the AMBER14 force field (Maier et al. 2015) and the md_run.mcr macro with default values in YASARA. The force field parameters for the heme molecule were applied as described earlier (Detzel et al. 2021). The results were analyzed using the md_analyze.mcr macro in YASARA. The final snapshot from the MD simulation was used as receptor in a set of focused molecular docking of heme molecule onto the histidine residues H^{236}, H^{238}, H^{260}, and H^{293}, respectively. In each run, a 15 Å cubic cell was defined around the histidine residue of interest as the docking search space. The resulting poses, filtered by the lowest histidine-iron-ion distance, were used for a 50 ns MD simulation using the Amber14 force field (Tian et al. 2020) in YASARA with the md_run.mcr macro with default values and heme as a ligand. A qualitative estimation of the heme-binding affinities on docked and MD-refined complexes were carried using the HYDE scoring function (Reulecke et al. 2008; Schneider et al. 2013), as implemented in the SeeSAR molecular modeling platform. Molecular graphics were created using SeeSAR (version 11.1.1; BioSolveIT GmbH, Sankt Augustin, Germany, 2021, www.biosolveit.de/SeeSAR), UCSF Chimera (version 1.13.1) (Pettersen et al. 2004), and YASARA (version 20.4.20) (Krieger and Vriend 2014).

Results and Discussion

Analytical Characteristics of the 66mer Hemopexin-Derived Peptide

The analytical data for the hemopexin-derived model peptide is provided in the supplemental information (Table S1; Fig. S1–S2). Amino acid analysis revealed a peptide content of 79.9%, which was considered for the concentration in all in vitro experiments herein.

Spectroscopic Studies of the Heme-Peptide/Hemopexin Complex

Currently, there is no experimentally determined structure available for the heme-bound full-length human hemopexin and respective histidine mutants. We thus characterized the heme binding to both, a 66mer hemopexin-derived peptide (P^{232} to I^{297}; Fig. 1A) and human hemopexin using spectroscopic methods to substantiate our hypothesis that more than one heme can bind to the protein (Detzel et al. 2021). The 66mer peptide was originally designed to include the heme-binding sites H^{236} and H^{293}, and the suggested H^{260} and H^{238} (Fig. 1A). In the recent report by Karnaukhova et al., induced CD changes (ICD) of the Soret band in a heme titration experiment were investigated (Karnaukhova

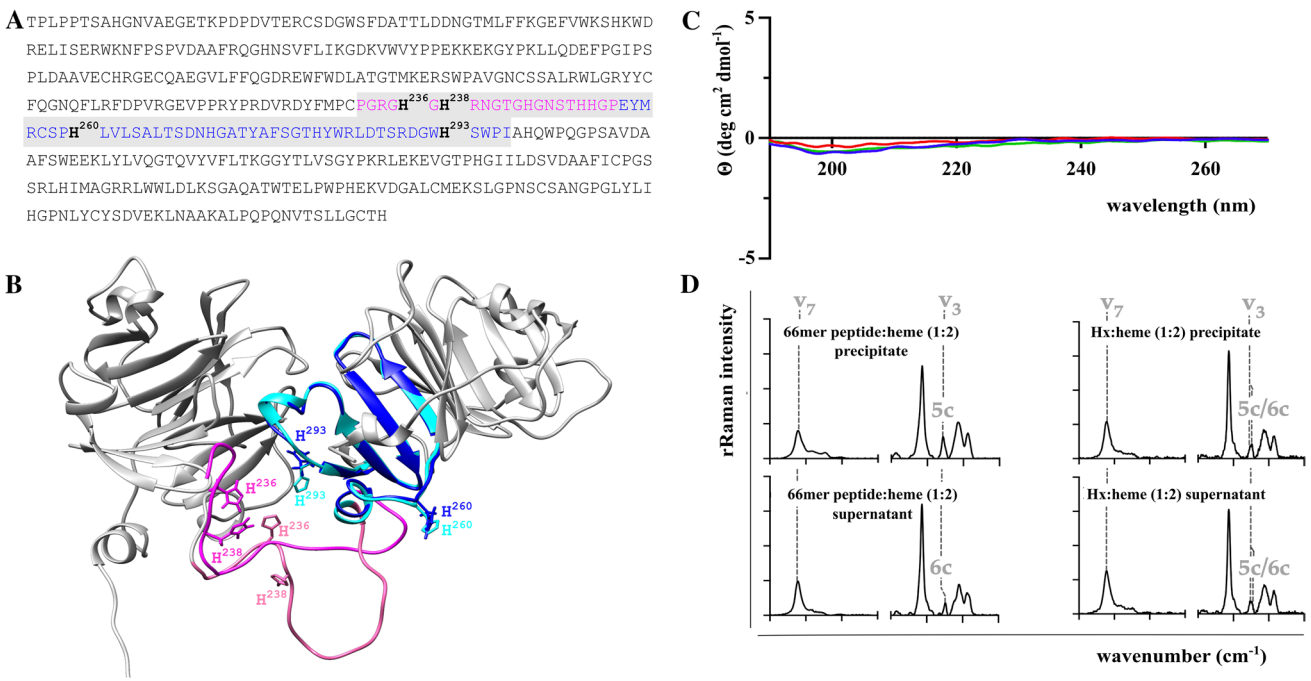

Fig. 1 **A** The hemopexin-derived 66mer peptide sequence (grey box) comprises the linker peptide (magenta) and a part of the sequence of the second β-propeller domain (blue) of wild-type mature hemopexin (complete sequence). The confirmed heme-binding sites H^{236} and H^{293} as well as the potential heme-binding sites H^{238} and H^{260} are highlighted (black bold). **B** The peptide shares the structural features of the C-terminal β-propeller domain (blue in peptide, turquoise in hemopexin) of full-length hemopexin (grey; homology model by AlphaFold 2 (https://alphafold.ebi.ac.uk/entry/P02790); signal peptide not entirely shown), whereas the N-terminus of the peptide (pink; derived from the linker peptide of hemopexin (rosa)) exhibits a high degree of flexibility. **C** CD spectra of the 66mer peptide (blue), the 66mer peptide-heme complex (1:1; red), and the 66mer peptide:heme complex (1:2; green). None of the spectra showed secondary structure elements possibly due to the high flexibility of the peptide. **D** Heme was added in a 1:2 (peptide/protein:heme) ratio to either the 66mer peptide or hemopexin and analyzed by rRaman spectroscopy. The spectral regions of interest (600–900 cm^{-1} and 1400–1800 cm^{-1}) are depicted. Upon complex formation, precipitation was observed. While the isolated precipitate contained heme complexed in the pentacoordinated (5c) state, there was evidence for a hexacoordinated (6c) state in the supernatant. In contrast, for the hemopexin-heme complex (1:2 ratio) mixed penta- and hexacoordination (5c/6c) was observed for both, the precipitate and the supernatant. *Hx* hemopexin

et al. 2021). Low heme concentrations provoked not only a monolobe Cotton effect CD spectrum at 420 nm, but an additional weak effect at 404 nm. Higher heme concentrations induced a bisignate ICD pattern, whose presence was attributed to exciton coupling between two at the same time hemopexin-bound heme molecules (Karnaukhova et al. 2021). The CD experiments performed in the present study were initiated to investigate conformational changes of the secondary structure elements of the 66mer peptide upon addition of heme [66mer peptide only, 66mer peptide:heme (1:1 and 1:2)]. This was based on the observation that the 66mer peptide adopts the same structural features as the respective part in full-length hemopexin (Fig. 1B). However, the 66mer peptide obviously exhibited too high flexibility, and thus, the CD signals were too low (< 1 θ) to calculate distinct changes in the secondary structure elements (Fig. 1C), preventing us from providing a CD study of the 66mer peptide. This means that heme binding to this anyways highly flexible part of hemopexin cannot stabilize the protein. Thus, rRaman experiments were performed instead to contribute to the analysis of a possible second heme-binding site in hemopexin using a different approach. The experimental setup was inspired by earlier investigations on heme-peptide/protein interactions (Kühl et al. 2013; Brewitz et al. 2016; Wißbrock et al. 2019a; Syllwasschy et al. 2020; Detzel et al. 2021), except that the hemopexin/66mer peptide-heme ratio was chosen as 1:2 for each interaction. Therefore, freshly prepared heme was added to the 66mer peptide and hemopexin, respectively, to avoid heme aggregation in aqueous solution during long-lasting in vitro rRaman experiments (Das et al. 1970; de Villiers et al. 2007). According to earlier studies concerning the analysis of the rRaman spectra (Spiro 1985; Wißbrock et al. 2019b), the iron coordination state can be derived from the $\nu 3$ band formed upon complex formation. Thereby, a pentacoordinated complex provokes a $\nu 3$ band at ~ 1491 cm^{-1} (Spiro 1985; Wißbrock et al. 2019b), whereas in case of a hexacoordinated complex this band appears at ~ 1505 cm^{-1} (Spiro and Burke 1976; Wißbrock et al. 2019b). Mixed complexes occur

as a double band, as can be seen in Fig. 1D (Kühl et al. 2013; Brewitz et al. 2016; Wißbrock et al. 2019a). The 1:2 (66mer peptide:heme) complex precipitated during the incubation time in the experiment. The same was observed for the proinflammatory cytokine interleukin-36α (IL-36α) and several other peptides (Brewitz et al. 2015; Wißbrock et al. 2019a). For IL-36α, two heme-binding sites could be confirmed, as well (Wißbrock et al. 2019a). This correlation prompted us to assume that the precipitation is a consequence of complex formation and does not result from heme aggregation. Hence, the supernatant and the resuspended precipitate were measured separately, yet under the same conditions. It was found that the precipitate represents a pentacoordinated complex (Fig. 1D), whereas in the supernatant a hexacoordinated complex was observed. This might indicate that the pentacoordinated complex precipitates, while the hexacoordinated remains soluble. It is highly probable that one heme molecule is hexacoordinated within the H^{236}/H^{293} binding cleft and the other bound to either H^{238} or H^{260}, resulting in a pentacoordinated state for the latter. Due to the unavailability of an experimentally determined structure of human hemopexin, evidence for a 1:1 binding could so far only be derived from the rabbit hemopexin structure (PDB ID: 1QJS) (Morgan and Müller-Eberhard 1972; Hrkal et al. 1974; Paoli et al. 1999). In our study, the heme-protein complex precipitated at a ratio of 1:2 (hemopexin:heme) under the conditions required for rRaman spectroscopy. Thus, the supernatant and the resuspended complex were again measured separately. Both fractions showed a mixed penta- and hexacoordination. In the protein context, and different from the situation of the 66mer peptide, these results could be interpreted as two different heme-binding sites: One representing the hexacoordinated heme-binding site H^{236}/H^{293} identified for the rabbit hemopexin (Paoli et al. 1999) and a second heme-binding site, which interacts with heme in a pentacoordinated fashion, i.e. either H^{79}, H^{238} or H^{260}. The latter two histidine residues were proposed by our HeMoQuest analysis (Paul George et al. 2020; Detzel et al. 2021) and were not considered as heme-binding sites in the literature so far, while H^{79} has been suggested as a heme-binding site by Satoh et al. (1994). H^{79}, however, has been earlier excluded due to its insufficient surface exposure, and H^{238} was considered unsuitable due to sterical hindrance (see below). In addition to the aforementioned scenario, H^{236} or H^{293} of another hemopexin molecule could coordinate heme in a pentacoordinated state (Fig. 1D), yet this is more likely at lower heme concentrations than at heme excess conditions. The heme recruitment mechanism could thus start with the binding of heme to H^{260}, which transfers it to the binding site H^{236}/H^{293} via a conformational change. The transfer, finally, releases the H^{260} binding site again and provides the same as a potential candidate for pentacoordination as the second binding event at high heme levels (Karnaukhova et al. 2014; Wißbrock et al. 2019a; Syllwasschy et al. 2020).

In Silico Study of the Free and Heme-Complexed 66mer Peptide by MD Simulation

The results of our recent in vitro study and a later submitted publication (Karnaukhova et al. 2021; Detzel et al. 2021) independently suggested higher hemopexin-heme binding ratios and a substantial conformational change after heme binding compared to earlier reports (Hrkal et al. 1974; Morgan et al. 1993; Satoh et al. 1994; Paoli et al. 1999). However, a clear structural proof can still not be given due to the limitations of the techniques used so far. A recently established model structure, initially predicted with SWISS-MODEL (Waterhouse et al. 2018; Detzel et al. 2021) of the 66mer peptide and the homology model of the human full-length protein (Detzel et al. 2021) were used to analyze the heme binding by molecular docking approaches, followed by molecular dynamics (MD) simulations, based on mutual comparison concerning structural stability and integrity. We recently could successfully support our in vitro findings via MD simulations with several peptides and proteins, and applied this method herein (Peherstorfer et al. 2018; Wißbrock et al. 2019a; Hopp et al. 2021; Detzel et al. 2021). The 66mer peptide was modeled with the pairwise structure-based MUSTANG alignment (Konagurthu et al. 2006) based on the available rabbit hemopexin structure (PDB ID: 1QJS) using YASARA (Paoli et al. 1999; Krieger and Vriend 2014; Detzel et al. 2021). An overlay of the 66mer peptide model structure with the full-length hemopexin homology model showed earlier high accuracy, with a backbone root-mean-square deviation (RMSD) of 0.772 Å (Detzel et al. 2021). The quality of our modelled structure was now additionally validated by comparing it against the full-length model of human hemopexin, which has recently been established by AlphaFold 2 (https://alphafold.ebi.ac.uk/entry/P02790) (Jumper et al. 2021; Varadi et al. 2022). A MUSTANG alignment of the 66mer peptide against the AlphaFold 2 structure as reference showed an RMSD of a meagre 0.92 Å, which was a strong indicator that we have an excellent model worthy of being subjected to additional computational experiments (Fig. 1B). The prime aim behind the computational efforts in this work was to retrospectively verify and visualize the hypotheses proposed by the experimental results of heme binding to the 66mer peptide. Therefore, to replicate a physiological environment, we subjected the peptide to a 2000 ns, explicit-solvent, all-atom MD simulation. This simulation provided a comprehensive idea of the conformational landscape that the peptide undergoes to get towards its stable folded conformation. The peptide underwent an

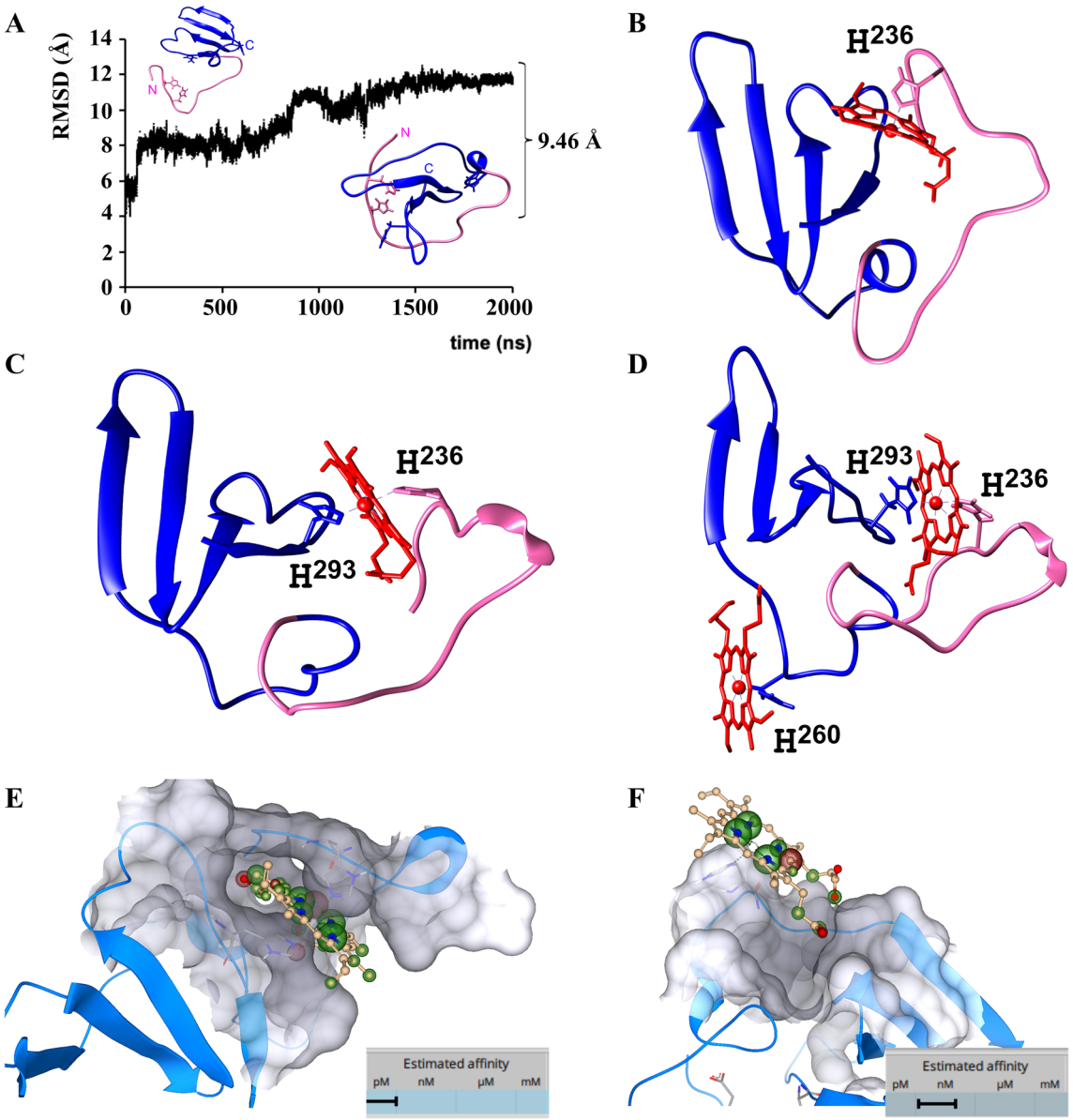

Fig. 2 **A** The overall backbone RMSD plot from a 2000 ns MD simulation of the hemopexin-derived peptide is depicted. A total change of ~ 9.46 Å has been recorded. The starting structure (left, above) and the final 2000 ns simulated structure (right, below) are shown as well. The parts derived from the hemopexin's linker peptide and from the C-terminal β-propeller domain are highlighted in magenta and blue, respectively. **B** Based on the in silico studies, binding to H^{236} is possible in a pentacoordinated fashion. **C** However, a bishistidyl heme hexacoordination by the earlier described residues H^{236} and H^{293} (Paoli et al. 1999) is only possible after structural rearrangement following the initial heme-binding event to H^{236}. **D** After structural incorporation of the heme molecule into the binding pocket of H^{235} and H^{293}, binding of a second heme molecule to H^{260} was observed. **E**, **F** Estimated by applying the HYDE scoring function in SeeSAR, the heme bound in a hexacoordinated state between H^{236} and H^{293} shows higher binding affinity (picomolar range) than the heme in pentacoordination to H^{260} (nanomolar range)

overall backbone RMSD change of 9.46 ± 1.64 Å (Fig. 2A). A large amount of the conformational change (~ 5 Å) was observed in the very first nanoseconds of the simulation as part of the solvent in the MD simulation equilibrating around the peptide, provoking this numerical bump in the RMSD value (Fig. 2A). Beyond this initial equilibration, the overall RMSD change of the peptide for the remainder of the simulation was gradual and the peptide settles in a stable conformation in the final 400 ns of the simulation with an RMSD of only 2.60 ± 0.30 Å. By the end of this simulation, the peptide attained a well-folded, compact conformation as indicated by the drop in the radius of gyration from 14.30 to 11.42 Å in the final snapshot. Interestingly, it is only towards the end of the simulation that the peptide sampled

conformations suitable for heme binding. The distance between the deprotonated nitrogen atoms of the residues H^{236} and H^{293} in the peptide was monitored over the course of the simulation, since it is assumed that these two residues bind heme in a hexacoordinated fashion. In the starting conformation of the simulation this distance was as large as 10.13 Å, which is a clear indicator that this conformation is not suited to bind heme especially in a hexacoordinated manner. Blind docking of heme on these initial conformations did not result in favorable heme-bound poses in any of the potential residues. In the final stages of the simulation (1500–2000 ns), when the peptide had equilibrated to sample a less diverse ensemble of conformations, this distance dropped drastically, maintaining an average distance of ~ 5 Å and going as low as 3.18 Å. Multiple structures from the last 500 ns of the trajectory were extracted and used as receptors for the docking of heme. Starting from these structures, heme binding to the peptide via H^{236} could be successfully modeled (Fig. 2B). However, at this stage the H^{293} residue, though still in the vicinity, was 7.16 Å away from iron ion of the heme molecule and the other side of the heme was coordinated by a water molecule from the MD system. Further conformational rearrangement was required to allow for hexacoordination. Thus, the peptide-heme complex (with heme bound to H^{236}) was subjected to an additional 50 ns all-atom MD simulation. Within the first 10 ns of this simulation, the heme–iron-H^{293} distance dropped dramatically and at around 18 ns, the H^{293} residue displaced the water molecule coordinating the heme iron and locked itself electrostatically onto the heme iron to form a perfectly hexacoordinated heme binding between H^{236} and H^{293} (Fig. 2C). On this complex (heme bound via H^{236} and H^{293}), an additional round of docking simulations was carried out to scan for further heme-binding sites on this complex. Interestingly, docked poses were clustered around the H^{260} residue with distances between the heme iron and the deprotonated nitrogen of the histidine residue less than 3 Å. A further round of energy minimization of the pose resulted in stabilizing the heme binding to H^{260} in a pentacoordinated manner (Fig. 2D). In order to qualitatively estimate the binding affinities of the two heme molecules bound in different regions of the peptide, the HYDE scoring function (Reulecke et al. 2008; Schneider et al. 2013) was used, as implemented in SeeSAR (version 11.1.1; BioSolveIT GmbH, Sankt Augustin, Germany, 2021, www.biosolveit.de/SeeSAR). The HYDE-estimated affinity for the heme molecule hexacoordinated between H^{236} and H^{293} was clearly much higher than the one that was pentacoordinated at H^{260}, clearly reflecting the trend observed in the experimental study (Fig. 2E, F). Our computational investigations have conclusively verified the earlier hypothesis that the 66mer sequence stretch derived from hemopexin can bind more than one heme molecule at the same time, and further confirmed the trend in binding quality between the two heme molecules with evidence from the modelled complexes. Although it should be emphasized that the peptide only represents a small part of the complete protein, it comprisesall earlier confirmed heme-binding motifs and seems to exhibit comparable folding to the corresponding sequence stretch in hemopexin. Together with our earlier results on the protein level (Detzel et al. 2021), it is highly probable that the herein proposed binding mechanism also applies to human full-length hemopexin. It is thus important to recognize the heme-binding capacity of the 66mer hemopexin-derived peptide for potential further use in drug research and development.

Conclusion

To gain additional structural insights into the heme-hemopexin interaction we herein applied spectroscopic and in silico techniques to analyze heme binding to a 66mer hemopexin-derived peptide (PGRG **H^{236}**G**H^{238}**RNGTGHGNSTHHGPEYMRCSP**H^{260}**LVLSALTSDNHGATYAFSGTHYWRLDTSRDGW**H^{293}**SWPI). Both, the 66mer peptide and the hemopexin protein, bind heme in mixed states of penta- and hexacoordination, as demonstrated by rRaman spectroscopy. The observed hexacoordinated binding mode confirms the bishistidyl heme binding between H^{236} and H^{293}, as earlier described for the crystal structure of rabbit hemopexin (Paoli et al. 1999). The pentacoordinated heme is highly probable binding to H^{260}. Beyond the earlier published (Detzel et al. 2021) and the herein reported experimental studies with hemopexin and the 66mer hemopexin-derived peptide, computational studies using the 66mer peptide now further supported the suggested heme recruitment mechanism for two heme molecules binding to hemopexin. Estimation of the heme-binding affinity to these sites revealed a significant higher heme-binding affinity for the bishistidyl binding site in comparison to H^{260}, providing further hints that, after the first heme molecule has been escorted to the hexacoordination site of H^{236} and H^{293}, residue H^{260} is again available for binding of the second heme molecule in pentacoordination. The herein described stepwise convoy of heme from H^{260} to H^{236} and H^{293} is also supported by the earlier described different heme-binding affinities of the respective HBMs (Detzel et al. 2021). Furthermore, this recruitment mechanism seems plausible if considering the recently described heme binding to the heme-degrading enzyme heme oxygenase-2, where heme is first bound to a surface-exposed HBM (C^{265}/H^{256} or C^{282}) and subsequently transferred into the core of the protein to H^{45} (Fleischhacker et al. 2020). Meanwhile, several proteins were identified to transiently bind more than one heme molecule (e.g., α1-microglobulin (Siebel et al. 2012), IL-36α (Wißbrock et al. 2019a), and activated protein C

(Hopp et al. 2021)). Thus, it might be interesting to follow whether other proteins will be added to this group of heme-binding proteins in the future.

Supplementary Information The online version contains supplementary material available at https://doi.org/10.1007/s10989-022-10441-x.

Acknowledgements The CD measurements were performed at the Protein Interaction Platform Cologne (http://PIPC.uni-koeln.de). The authors would like to thank Dr. Benjamin F. Schmalohr and Aya S. M. Abdelbaky (University of Bonn) for technical assistance.

Author contribution Conceptualization, DI; methodology, MTH, AAPG, AP, AR, and MSD; software, AAPG; data curation, MTH, AAPG, AP, and AR; writing—original draft preparation, DI, MTH, AAPG, and MSD; writing—review and editing, DI and MTH; visualization, MTH, AAPG; supervision, DI and UN; project administration, DI. All authors have read and agreed to the published version of the manuscript.

Funding Open Access funding enabled and organized by Projekt DEAL.

Declarations

Conflict of interests The authors declare that they have no financial interests.

References

Belcher JD, Chen C, Nguyen J et al (2018) Haptoglobin and hemopexin inhibit vaso-occlusion and inflammation in murine sickle cell disease: role of heme oxygenase-1 induction. PLoS ONE 13:e0196455. https://doi.org/10.1371/journal.pone.0196455

Brewitz HH, Kühl T, Goradia N et al (2015) Role of the chemical environment beyond the coordination site: structural insight into Fe(III)protoporphyrin binding to cysteine-based heme-regulatory protein motifs. ChemBioChem 16:2216–2224. https://doi.org/10.1002/cbic.201500331

Brewitz HH, Goradia N, Schubert E et al (2016) Heme interacts with histidine- and tyrosine-based protein motifs and inhibits enzymatic activity of chloramphenicol acetyltransferase from *Escherichia coli*. Biochim Biophys Acta - Gen Subj 1860:1343–1353. https://doi.org/10.1016/j.bbagen.2016.03.027

Buehler PW, Swindle D, Pak DI et al (2021) Hemopexin dosing improves cardiopulmonary dysfunction in murine sickle cell disease. Free Radic Biol Med 175:95–107. https://doi.org/10.1016/j.freeradbiomed.2021.08.238

Buzzi RM, Akeret K, Schwendinger N et al (2021) Spatial transcriptome analysis defines heme as a hemopexin-targetable inflammatoxin in the brain. Free Radic Biol Med. https://doi.org/10.1016/j.freeradbiomed.2021.11.011

Chen-Roetling J, Li Y, Cao Y et al (2021) Effect of hemopexin treatment on outcome after intracerebral hemorrhage in mice. Brain Res 1765:147507. https://doi.org/10.1016/j.brainres.2021.147507

Das RR, Pasternack RF, Plane RA (1970) Fast reaction kinetics of porphyrin dimerization in aqueous solution. J Am Chem Soc 92:3312–3316. https://doi.org/10.1021/ja00714a013

de Villiers KA, Kaschula CH, Egan TJ, Marques HM (2007) Speciation and structure of ferriprotoporphyrin IX in aqueous solution: spectroscopic and diffusion measurements demonstrate dimerization, but not μ-oxo dimer formation. JBIC J Biol Inorg Chem 12:101–117. https://doi.org/10.1007/s00775-006-0170-1

Detzel MS, Schmalohr BF, Steinbock F et al (2021) Revisiting the interaction of heme with hemopexin. Biol Chem 402:675–691. https://doi.org/10.1515/hsz-2020-0347

Dutra FF, Alves LS, Rodrigues D et al (2014) Hemolysis-induced lethality involves inflammasome activation by heme. Proc Natl Acad Sci 111:E4110–E4118. https://doi.org/10.1073/pnas.1405023111

Fleischhacker AS, Gunawan AL, Kochert BA et al (2020) The heme-regulatory motifs of heme oxygenase-2 contribute to the transfer of heme to the catalytic site for degradation. J Biol Chem 295:5177–5191. https://doi.org/10.1074/jbc.RA120.012803

Frimat M, Boudhabhay I, Roumenina LT (2019) Hemolysis derived products toxicity and endothelium: model of the second hit. Toxins (basel) 11:660. https://doi.org/10.3390/toxins11110660

Hopp M-T, Imhof D (2021) Linking labile heme with thrombosis. J Clin Med 10:427. https://doi.org/10.3390/jcm10030427

Hopp M-T, Schmalohr BF, Kühl T et al (2020) Heme determination and quantification methods and their suitability for practical applications and everyday use. Anal Chem 92:9429–9440. https://doi.org/10.1021/acs.analchem.0c00415

Hopp M-T, Alhanafi N, Paul George AA et al (2021) Molecular insights and functional consequences of the interaction of heme with activated protein C. Antioxid Redox Signal 34:32–48. https://doi.org/10.1089/ars.2019.7992

Hrkal Z, Vodrazka Z, Kalousek I (1974) Transfer of heme from ferrihemoglobin and ferrihemoglobin isolated chains to hemopexin. Eur J Biochem 43:73–78. https://doi.org/10.1111/j.1432-1033.1974.tb03386.x

Hvidberg V, Maniecki MB, Jacobsen C et al (2005) Identification of the receptor scavenging hemopexin-heme complexes. Blood 106:2572–2579. https://doi.org/10.1182/blood-2005-03-1185

Jumper J, Evans R, Pritzel A et al (2021) Highly accurate protein structure prediction with AlphaFold. Nature 596:583–589. https://doi.org/10.1038/s41586-021-03819-2

Karnaukhova E, Rutardottir S, Rajabi MM et al (2014) Characterization of heme binding to recombinant α1-microglobulin. Front Physiol 5:465. https://doi.org/10.3389/fphys.2014.00465

Karnaukhova E, Owczarek C, Schmidt P et al (2021) Human plasma and recombinant hemopexins: heme binding revisited. Int J Mol Sci 22:1199. https://doi.org/10.3390/ijms22031199

Konagurthu AS, Whisstock JC, Stuckey PJ, Lesk AM (2006) MUSTANG: a multiple structural alignment algorithm. Proteins Struct Funct Bioinforma 64:559–574. https://doi.org/10.1002/prot.20921

Krieger E, Vriend G (2014) YASARA View - molecular graphics for all devices—from smartphones to workstations. Bioinformatics 30:2981–2982. https://doi.org/10.1093/bioinformatics/btu426

Kühl T, Sahoo N, Nikolajski M et al (2011) Determination of hemin-binding characteristics of proteins by a combinatorial peptide

library approach. ChemBioChem 12:2846–2855. https://doi.org/10.1002/cbic.201100556
Kühl T, Wißbrock A, Goradia N et al (2013) Analysis of Fe(III) heme binding to cysteine-containing heme-regulatory motifs in proteins. ACS Chem Biol 8:1785–1793. https://doi.org/10.1021/cb400317x
Kumar S, Bandyopadhyay U (2005) Free heme toxicity and its detoxification systems in human. Toxicol Lett 157:175–188. https://doi.org/10.1016/j.toxlet.2005.03.004
Maier JA, Martinez C, Kasavajhala K et al (2015) ff14SB: improving the accuracy of protein side chain and backbone parameters from ff99SB. J Chem Theory Comput 11:3696–3713. https://doi.org/10.1021/acs.jctc.5b00255
Morgan WT, Müller-Eberhard U (1972) Interactions of porphyrins with rabbit hemopexin. J Biol Chem 247:7181–7187
Morgan WT, Heng Liem H, Sutor RP, Muller-Eberhard U (1976) Transfer of heme from heme-albumin to hemopexin. Biochim Biophys Acta - Gen Subj 444:435–445. https://doi.org/10.1016/0304-4165(76)90387-1
Morgan WT, Muster P, Tatum F et al (1993) Identification of the histidine residues of hemopexin that coordinate with heme-iron and of a receptor-binding region. J Biol Chem 268:6256–6262
Paoli M, Anderson BF, Baker HM et al (1999) Crystal structure of hemopexin reveals a novel high-affinity heme site formed between two beta-propeller domains. Nat Struct Biol 6:926–931. https://doi.org/10.1038/13294
Paul George AA, Lacerda M, Syllwasschy BF et al (2020) HeMoQuest: a webserver for qualitative prediction of transient heme binding to protein motifs. BMC Bioinf 21:124. https://doi.org/10.1186/s12859-020-3420-2
Peherstorfer S, Brewitz HH, Paul George AA et al (2018) Insights into mechanism and functional consequences of heme binding to hemolysin-activating lysine acyltransferase HlyC from Escherichia coli. Biochim Biophys Acta 1862:1964–1972. https://doi.org/10.1016/j.bbagen.2018.06.012
Peters T (1996) All about albumin—biochemistry, genetics, and medical applications. Academic Press Inc., San Diego
Pettersen EF, Goddard TD, Huang CC et al (2004) UCSF Chimera—a visualization system for exploratory research and analysis. J Comput Chem 25:1605–1612. https://doi.org/10.1002/jcc.20084
Poillerat V, Gentinetta T, Leon J et al (2020) Hemopexin as an inhibitor of hemolysis-induced complement activation. Front Immunol 11:1684. https://doi.org/10.3389/fimmu.2020.01684
Reulecke I, Lange G, Albrecht J et al (2008) Towards an integrated description of hydrogen bonding and dehydration: decreasing false positives in virtual screening with the HYDE scoring function. ChemMedChem 3:885–897. https://doi.org/10.1002/cmdc.200700319
Roumenina LT, Rayes J, Lacroix-Desmazes S, Dimitrov JD (2016) Heme: modulator of plasma systems in hemolytic diseases. Trends Mol Med 22:200–213. https://doi.org/10.1016/j.molmed.2016.01.004
Ryan CG, Clayton E, Griffin WL et al (1988) SNIP, a statistics-sensitive background treatment for the quantitative analysis of PIXE spectra in geoscience applications. Nucl Instrum Methods Phys Res Sect B 34:396–402. https://doi.org/10.1016/0168-583X(88)90063-8
Satoh T, Satoh H, Iwahara S et al (1994) Roles of heme iron-coordinating histidine residues of human hemopexin expressed in baculovirus-infected insect cells. Proc Natl Acad Sci 91:8423–8427. https://doi.org/10.1073/pnas.91.18.8423
Schneider N, Lange G, Hindle S et al (2013) A consistent description of HYdrogen bond and DEhydration energies in protein–ligand complexes: methods behind the HYDE scoring function. J Comput Aided Mol Des 27:15–29. https://doi.org/10.1007/s10822-012-9626-2
Siebel JF, Kosinsky RL, Åkerström B, Knipp M (2012) Insertion of heme b into the structure of the Cys34-carbamidomethylated human lipocalin α1-microglobulin: formation of a [(heme)2(α1-microglobulin)]3 complex. ChemBioChem 13:879–887. https://doi.org/10.1002/cbic.201100808
Smith A, Morgan WT (1981) Hemopexin-mediated transport of heme into isolated rat hepatocytes. J Biol Chem 256:10902–10909. https://doi.org/10.1016/S0021-9258(19)68530-3
Spiro TG, Burke JM (1976) Protein control of porphyrin conformation. Comparison of resonance Raman spectra of heme proteins with mesoporphyrin IX analogs. J Am Chem Soc 98:5482–5489. https://doi.org/10.1021/ja00434a013
Syllwasschy BF, Beck MS, Družeta I et al (2020) High-affinity binding and catalytic activity of His/Tyr-based sequences: extending heme-regulatory motifs beyond CP. Biochim Biophys Acta - Gen Subj 1864:129603. https://doi.org/10.1016/j.bbagen.2020.129603
Takahashi N, Takahashi Y, Putnam FW (1985) Complete amino acid sequence of human hemopexin, the heme-binding protein of serum. Proc Natl Acad Sci 82:73–77. https://doi.org/10.1073/pnas.82.1.73
Tian C, Kasavajhala K, Belfon KAA et al (2020) ff19SB: Amino-acid-specific protein backbone parameters trained against quantum mechanics energy surfaces in solution. J Chem Theory Comput 16:528–552. https://doi.org/10.1021/acs.jctc.9b00591
Tolosano E, Altruda F (2002) Hemopexin: Structure, function, and regulation. DNA Cell Biol 21:297–306. https://doi.org/10.1089/104454902753759717
Tolosano E, Fagoonee S, Morello N et al (2010) Heme scavenging and the other facets of hemopexin. Antioxid Redox Signal 12:305–320. https://doi.org/10.1089/ars.2009.2787
Varadi M, Anyango S, Deshpande M et al (2022) AlphaFold protein structure database: massively expanding the structural coverage of protein-sequence space with high-accuracy models. Nucleic Acids Res 50:D439–D444. https://doi.org/10.1093/nar/gkab1061
Waterhouse A, Bertoni M, Bienert S et al (2018) SWISS-MODEL: homology modelling of protein structures and complexes. Nucleic Acids Res 46:W296–W303. https://doi.org/10.1093/nar/gky427
Wißbrock A, Goradia NB, Kumar A et al (2019a) Structural insights into heme binding to IL-36α proinflammatory cytokine. Sci Rep 9:16893. https://doi.org/10.1038/s41598-019-53231-0
Wißbrock A, Paul George AA, Brewitz HH et al (2019b) The molecular basis of transient heme-protein interactions: analysis, concept and implementation. Biosci Rep 39:BSR20181940. https://doi.org/10.1042/BSR20181940
R Core Team (2021) R: a language and environment for statistical computing. https://www.r-project.org. Accessed 18 Apr 2021
Spiro TG (1985) Resonance Raman spectroscopy as a probe of heme protein structure and dynamics. In: Advances in protein chemistry. pp 111–159